# Uniplanar oriented isotactic polypropylene: 3. Properties and morphology

**Satoshi Osawa* and Roger S. Porter†**
*Polymer Science and Engineering Department, University of Massachusetts, Amherst, MA 01003, USA*

**and Masayoshi Ito**
*Department of Chemistry, Science University of Tokyo, Kagurazaka, Shinjuku-ku, Tokyo 162, Japan*
*(Received 26 March 1993; revised 8 May 1993)*

Isotactic polypropylene was uniaxially compressed by a forging (uniplanar) process. The physical properties and morphology of the compressed samples were investigated by means of mechanical tests, trirefringence measurement and microscopy. Four major effects of planar deformation on the physical properties and morphology were observed. (1) The glass transition temperature of the compressed sample (evaluated from dynamic mechanical analysis) increased with draw. (2) The smectic phase induced by the compression draw increased sample transparency. (3) Both tensile modulus and strength parallel to the uniplanar direction increased with draw. The smectic phase generated, however, reduced the tensile modulus with no significant effect on tensile strength. (4) The compressed samples possessed a layered structure which was developed by the flattening of the original spherulites.

**(Keywords: planar deformation; isotactic polypropylene; morphology)**

## INTRODUCTION

Attention has been focused on the physical properties of uniaxially oriented thermoplastics[1,2]. Among the polymers studied, isotactic polypropylene (i-PP) has been drawn uniaxially to high levels[3–5]. Although biaxially oriented thermoplastics are important for their enhanced in-plane properties[6–18], relatively little information on the structure and properties of i-PP have been reported[19–22].

By applying a forging (uniplanar or pseudo-equibiaxial) process, we have previously[23] drawn i-PP up to a compression ratio (CR) of 50 ($7.1 \times 7.1$). It has been reported[24,25] that the orientation function of uniaxially drawn i-PP crystals increases rapidly up to a draw ratio of 8–10, before levelling off. Although the highest draw ratio for the planar direction of our forged samples (7.1) is lower than 8–10, this value is high for chain orientation in the planar direction. We found[23] that the major structural change of forged i-PP appears below a compression ratio of about 10 ($3.2 \times 3.2$). For example, the amorphous density increases with compression draw up to CR $\approx$ 10, and the fraction of smectic phase caused by the compression draw (at 50°C) increases rapidly with CR up to 5 ($2.2 \times 2.2$).

In this study, the physical properties and morphology of the compressed i-PP have been examined by using mechanical tests, trirefringence measurement and microscopy. The results are discussed with the previous structural study of biaxially oriented i-PP[23].

## EXPERIMENTAL

Moulded i-PP sheet was uniaxially compressed under a constant compression speed of 0.254 cm min$^{-1}$ by using an Instron model 1333, which allows on-line measurement of load and displacement during the deformation process. A detailed description of the i-PP and the compression test have been given previously[23,26,27].

The refractive index in the film plane and thickness direction were measured using an Abbe refractometer with a rotatable light polarizer mounted on the eye piece[28]. To avoid surface scattering, 1-bromonaphthalate (refractive index of 1.6576 at 20°C) was used as an immersion fluid. The prisms and sample were maintained at 21°C by circulating water through the refractometer via a constant-temperature bath. *Figure 1* shows the geometry for the measurement. The $Z$-axis is parallel to the compression direction and the $X$–$Y$ plane is parallel to the sample surface. Dynamic mechanical

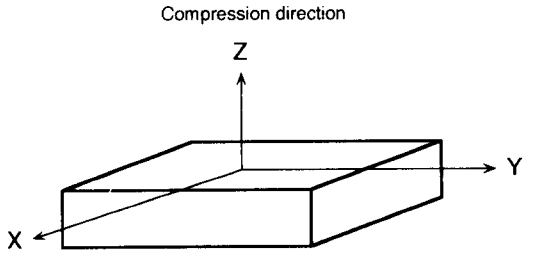


**Figure 1** Sample geometry for trirefringence and mechanical tests. The $Z$-axis is the compression direction and the $X$–$Y$ plane is parallel to the sample surface (plane direction)

* Present address: Department of Materials Science and Technology, Science University of Tokyo, Yamaguchi College, Daigakudori, Onodashi, Yamaguchi 756, Japan
† To whom correspondence should be addressed

0032-3861/94/030551-07

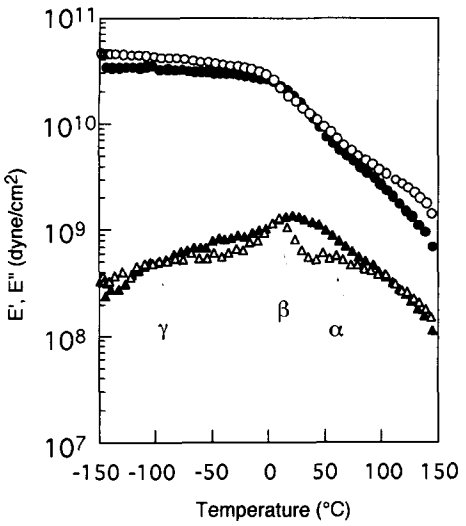


**Figure 2** Dynamic storate ($E'$; ○, ●) and loss ($E''$; △, ▲) modulus at 11 Hz as a function of temperature for the compressed sample (50°C, CR = 10; solid symbols) and the original sample (open symbols)

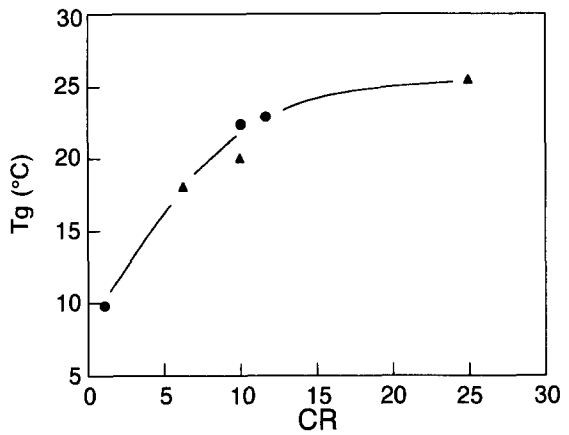


**Figure 3** $T_g$ evaluated from the peak temperature of $\beta$ relaxation as a function of CR for samples compressed at 50°C (●) and 100°C (▲)

measurements (stretching mode) were performed on a Rheovibron (Orientec Co.) at 11 Hz in the range −150 to 150°C. The samples (2 cm long and 2 mm wide) for these measurements were cut from compressed circular films. The tensile modulus and strength of the samples were measured at room temperature and at a strain rate of $1 \times 10^{-3}$ and $1 \times 10^{-2}\,s^{-1}$, respectively. Thermal analyses were performed on a Perkin–Elmer DSC 7 calorimeter. All scans were recorded at a heating rate of 20°C $min^{-1}$. Density measurements were made on a density gradient column, using ethyl alcohol and water as a mixed miscible solvent pair.

## RESULTS AND DISCUSSION

### *Glass transition temperature*

*Figure 2* shows storage ($E'$) and loss ($E''$) tensile moduli measured at 11 Hz as a function of temperature for the compressed sample (50°C, CR = 10) and the original undeformed samples. Three main relaxations, labelled $\alpha$, $\beta$ and $\gamma$, are identified in the figure. The intermediate $\beta$ peak at about 10°C was found to be intense and was identified with the glass transition temperature, $T_g$[29,30]. The $\gamma$ and $\alpha$ relaxations were weak or absent, as attributed to the local motions in the amorphous fraction[31] and relaxation of crystal[32,33], respectively. The $\beta$ peak temperature increased with draw. This means that $T_g$ is increased by the compression draw. From the $\beta$ relaxation, $T_g$ can be evaluated as a function of CR. These results are shown in *Figure 3*. $T_g$ increases steeply from 9°C for the original undrawn sample to 23°C for the sample drawn at CR = 10, followed by a gradual increase. We have shown[23] that the amorphous density increases with compression draw, i.e. the same trend as seen in *Figure 3*. The increase in $T_g$ appears to be associated with the increase in amorphous density on draw.

A rough estimation of $T_g$ shift ($\Delta T_g$) with increase in amorphous density has been carried out by using a simple Simha and Boyer model[34,35] (*Figure 4*):

$$V_g(T) = E_g T + V_g(0) \quad (1)$$

$$V_l(T) = E_l T + V_c(0) \quad (2)$$

$$V'_g(T) = E_g T + V_c(0) - \Delta V_g \quad (3)$$

$$V'_l(T) = E_l T + V_c(0) - \Delta V_l \quad (4)$$

where $V(T)$ is molar volume at $T$(K), $E$ is molar thermal expansion and the subscriptions c, g and l represent crystal, glass and undercooling liquid state, respectively. $V'_g(T)$ and $V'_l(T)$ are the molar volume of compressed sample for glassy and undercooled state, respectively. $\Delta V_g$ and $\Delta V_l$ are the difference of molar volume between original (uncompressed) and compressed sample for the glassy and undercooling liquid states, respectively. The $V_l(T)$ for the original (uncompressed) sample was changed by $\Delta V_l$ (0.7 $cm^3\,mol^{-1}$)[23] at CR = 25. On compression, $T_g$ of the sample increased from 9°C (for original) to 25°C (for CR = 25); $\Delta T_g = 16$°C. If $V'_l(T)$ for the compressed sample obeys equation (4), equations (3) and (4) are assumed to be equal at $T_{g2}$ ($T_g$ of compressed sample). At $T_{g1}$ ($T_g$ of uncompressed sample), equations (1) and (2) are assumed to be equal. Therefore, the $T_g$ shift

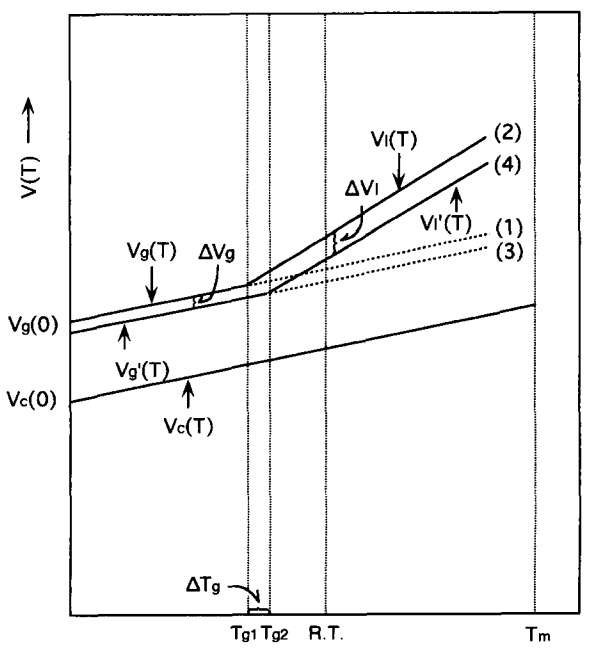


**Figure 4** Thermal expansion model of polymers (based on Simha and Boyer[34] model). Lines (1) to (4) correspond to equations (1) to (4), respectively

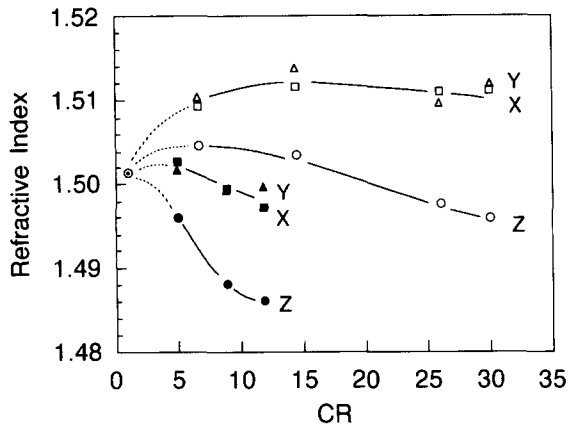


**Figure 5** Refractive indices of three mutually perpendicular directions as a function of CR for samples prepared at 50°C (●, $N_z$; ▲, $N_y$; ■, $N_x$) and 140°C (○, $N_z$; △, $N_y$; □, $N_x$) and original (⊙). The sample geometry is shown in *Figure 1*

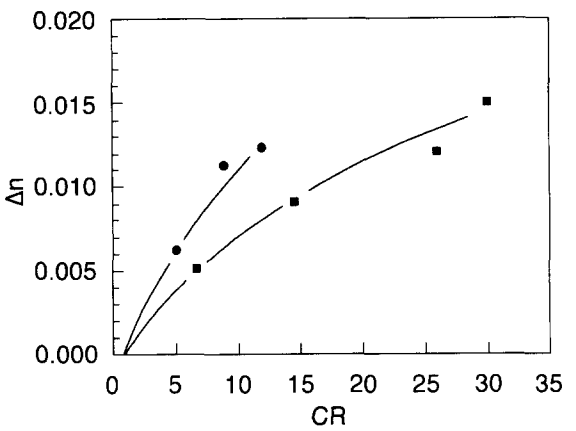


**Figure 6** Average birefringence, $\Delta n = 1/2(N_x + N_y) - N_z$, as a function of CR for samples prepared at 50°C (●) and 140°C (■)

$(T_{g2} - T_{g1} = \Delta T_g)$ is expressed by:

$$\Delta T_g = \frac{\Delta V_1 - \Delta V_g}{E_1 - E_g} \tag{5}$$

If $\Delta V_g = 0$ ($\Delta V_g$ is unknown but $\Delta V_1 \geqslant \Delta V_g$), equation (5) gives $\Delta T_g$. Taking[35] $E_1 = (232\text{–}396) \times 10^{-4}$ cm$^3$ mol$^{-1}$ K$^{-1}$ and $E_g = 93 \times 10^{-4}$ cm$^3$ mol$^{-1}$ K$^{-1}$, then the $\Delta T_g$ is calculated to be 23–50°C. The observed $\Delta T_g$ of 16°C is lower than this rough calculation. The increase in $T_g$ is attributable to the increase in amorphous density caused by the compression. The increase in $T_g$ of i-PP by the uniplanar deformation contrasts with the decrease noted on uniaxial deformation[29,36].

*Refractive index*

Trirefringence measurements were performed on the compressed samples. *Figure 5* shows refractive indices, $N$, of samples for the three principal directions. After compression at 140°C, the sample consists of amorphous phase plus the α-crystal phase. After compression at 50°C, the smectic phase is observed in addition[23]. For both temperatures, $N_x \approx N_y$, which indicates orientation symmetry around the $Z$-direction. Further, $N_x$ and $N_y$ are greater than $N_z$, confirming that the chain orientation is in the plane normal to the $Z$-axis. Because the forging is an equibiaxial process, ideally $\Delta xz = N_x - N_z$ and $\Delta yz = N_y - N_z$ should be the same. To evaluate planar orientation, $\Delta n = 1/2(N_x + N_y) - N_z$ is chosen as an average birefringence. *Figure 6* shows the plots of $\Delta n$ as a function of CR for samples compressed at 140 and 50°C. The $\Delta n$ increased with draw for both temperatures. Further, $\Delta n$ for 50°C is higher than that for 140°C at a given CR. This suggests that overall draw efficiency is higher at lower draw temperature, if the intrinsic birefringence of smectic and α-crystal phases is comparable. The $\Delta n$ for 140°C agrees with that of simultaneously biaxially drawn i-PP at 150°C (ref. 19). The relation between planar orientation and mechanical properties is discussed below.

The three mutually perpendicular refractive indices for uniaxially drawn i-PP have been studied by Samuels and co-workers[28,37]. They showed that $N_x$ and $N_y$ increased and $N_z$ decreased symmetrically with draw (where $N_z$ in *Figure 1* is uniaxial draw direction). For our uniplanar drawn sample in *Figure 5*, the refractive index for every direction tends to decrease with CR (but the $\Delta n$ increases with draw). This suggests that the average refractive index of the sample decreases with draw. The average refractive index, $N$, is expressed by the average of the refractive indices for three mutually perpendicular directions[28]:

$$\bar{N} = (N_x + N_y + N_z)/3 \tag{6}$$

Equation (6) is applicable for all samples with different CR, because of its independence of orientation. The $\bar{N}$ of the mixture is also related to the volume fraction for each of the components:

$$\bar{N} = \sum_i N_i V_i \tag{7}$$

where subscript $i$ represents the $i$th phase, $V_i$ is the volume fraction of $i$ phase and $\sum V_i = 1$. Because the volume fraction $V_i$ is related to weight fraction $X_i$ with $V_i = X_i(\rho/\rho_i)$, where $\rho$ is sample density and $\rho_i$ is $i$th phase density, equation (7) can be rewritten as:

$$\bar{N} = \sum_i N_i X_i \frac{\rho}{\rho_i} \tag{8}$$

From equation (8), the average refractive index is proportional to the sample density. Indeed, *Figure 7* shows the linear relationship of $\bar{N}$ with sample density. These data match the dashed line for undrawn samples of different crystallinity[28]. Sample density decreases with compression draw[23] (amorphous density increases,

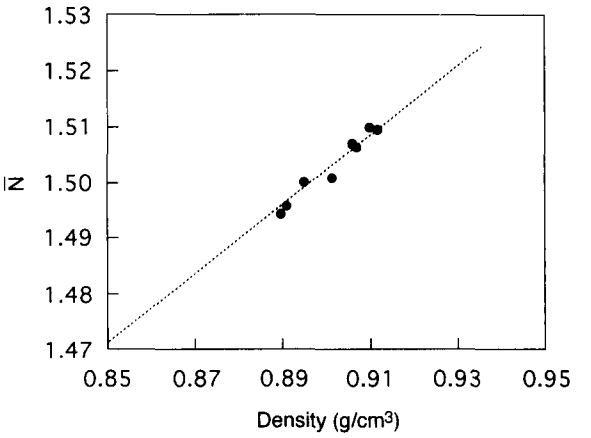


**Figure 7** Relation between the average refractive index, $\bar{N}$, and the sample density

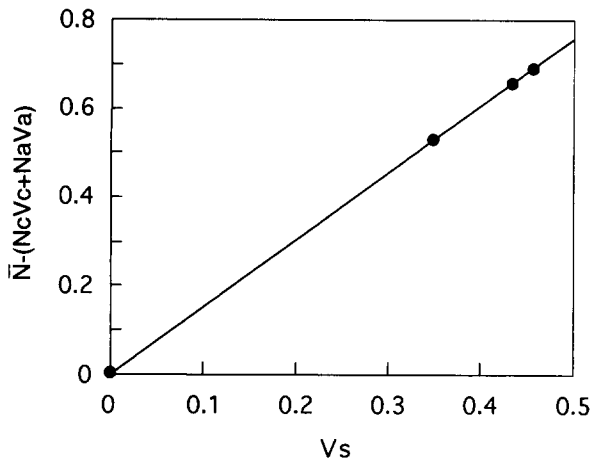


**Figure 8** $\bar{N}-(N_cV_c+N_aV_a)$ *versus* volume fraction of smectic phase, $V_s$

**Table 1** Volume fraction of each phase ($V$), sample density ($\rho$), average refractive index ($\bar{N}$) and average birefringence ($\Delta n$) for samples compressed at 50°C with different compression ratios (CR)

| CR | $V_s$ | $V_a$ | $V_c$ | $\rho$ (g cm$^{-3}$) | $\bar{N}$ | $\Delta n$ ($\times 10^3$) |
|---|---|---|---|---|---|---|
| 5.0 | 0.348 | 0.389 | 0.262 | 0.895 | 1.5001 | 6.2 |
| 8.9 | 0.434 | 0.447 | 0.120 | 0.891 | 1.4956 | 11.3 |
| 11.9 | 0.457 | 0.474 | 0.070 | 0.889 | 1.4943 | 12.4 |

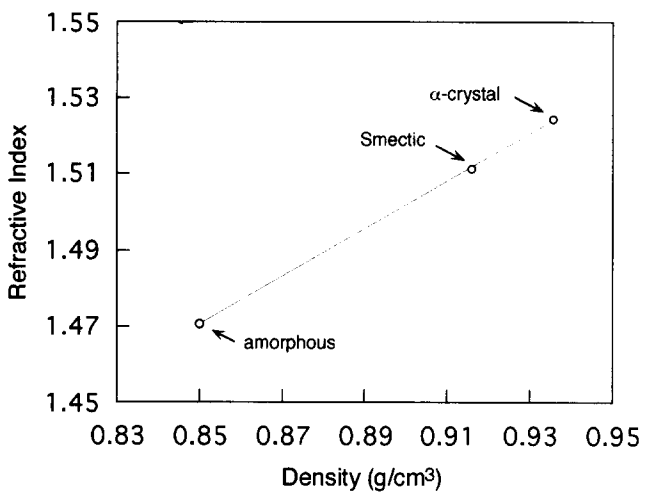


**Figure 9** Relation between the refractive index of each phase and phase density

but sample density decreases due to the decrease in crystallinity with compression draw). Therefore, the decrease in $N$ with draw in *Figure 5* is attributed to the decrease in sample crystallinity.

For deformation at 50°C, the compressed sample has α-crystal, smectic and amorphous phases. In this case, equation (7) gives:

$$\bar{N}=N_cV_c+N_aV_a+N_sV_s \quad (9)$$

where subscripts c, a and s represent crystal, amorphous and smectic phases, respectively. From a slope for the plots of $\bar{N}-(N_cV_c+N_aV_a)$ against $V_a$ (*Figure 8*), $N_s$ can be calculated. In the previous study, we evaluated the fraction of each phase for the same compression sample in this work[23]. Based on this procedure, the fraction of each phase is estimated (*Table 1*). By using $N_c=1.5245$ (density, $d=0.936$ g cm$^{-3}$), $N_a=1.4707$ ($d=0.850$ g cm$^{-3}$) from ref. 28, then $N_s$ is estimated to be 1.512 ($d=0.916$ g cm$^{-3}$)[38]. The relation of refractive index for each phase to phase density is shown in *Figure 9*. For 50°C, α-crystals transform to smectic phase on draw. Further, amorphous density increases. The difference in refractive index of smectic and amorphous phases is closer than that of α-crystal and amorphous phases. This markedly influences the optical properties of the compression sample. *Figure 10* shows that the transparency of compressed samples is improved by the compression draw. The increase in amorphous density and formation of smectic phase by compression draw reduces light scattering of the sample.

*Mechanical properties*

Forging induces equibiaxial deformation. The chains orient in the plane direction. Thus mechanical properties for every direction in the plane perpendicular to compression direction should be equal and should be enhanced by the draw. *Figure 11* shows tensile moduli in the plane direction for compressed samples as a function of CR. For 100 and 140°C (sample consists of α-crystal and amorphous phases), the modulus increases monotonically with CR. The highest value of 3.3 GPa at CR = 43 (6.6 × 6.6) is comparable to that of simultaneously biaxially drawn i-PP[19]. However, these values are lower than that of uniaxially drawn i-PP at a comparable draw ratio of 6 (refs 3, 39) as found for biaxially drawn polyethylene film[10]. For 50°C, the modulus decreases up to CR ≈ 5 followed by an increase,

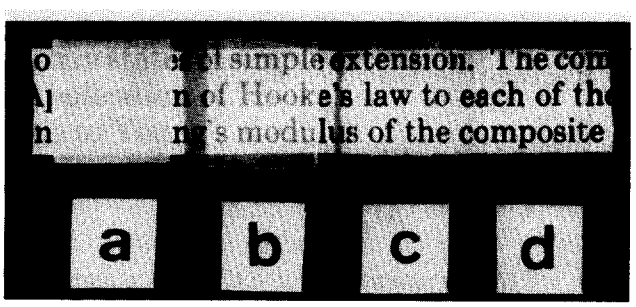


**Figure 10** Photograph of compressed i-PP samples deformed at 50°C at CR values of (a) 1.5; (b) 2.3; (c) 3.7; (d) 11.4

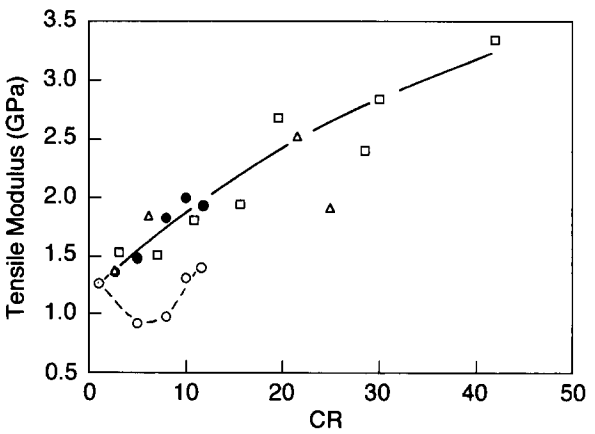


**Figure 11** Tensile modulus *versus* CR for samples prepared at 50°C (○), 100°C (△) and 140°C (□), and 50°C sample subsequently heat treated at 140°C for 30 min (●)

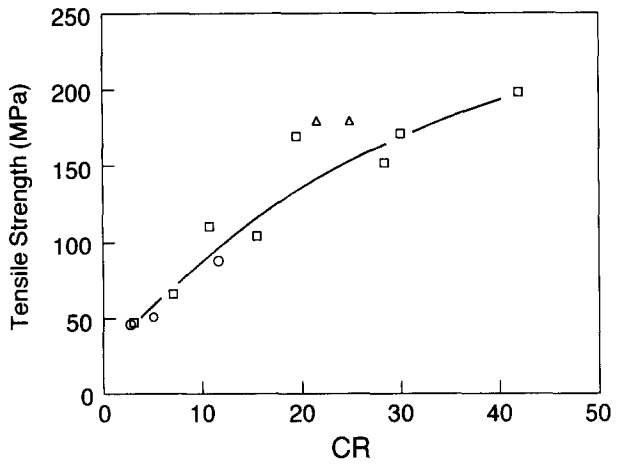


**Figure 12** Tensile strength *versus* CR for samples prepared at 50°C (○), 100°C (△) and 140°C (□)

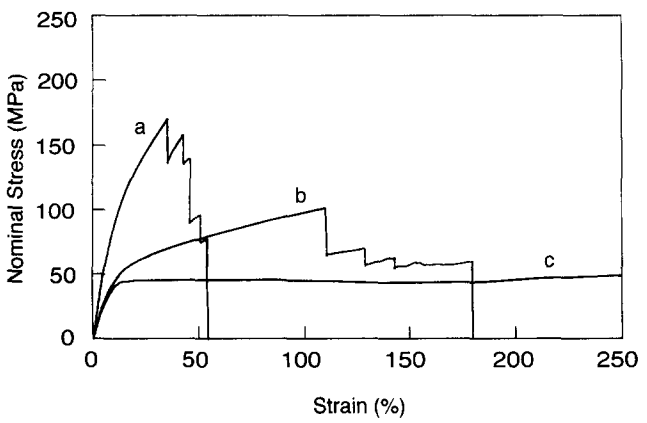


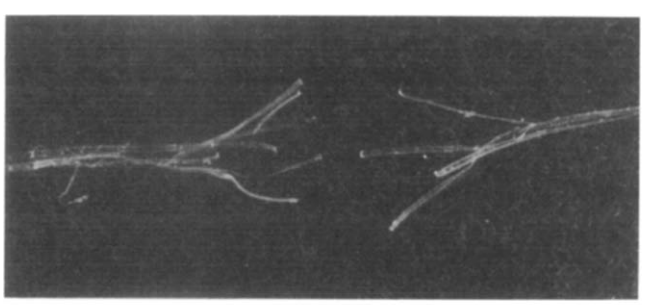

**Figure 13** Nominal stress–strain curves along plane direction for samples prepared at 140°C with CR of 30 (a), 11 (b) and original (c). The photograph shows the sample with CR = 30 after fracture

although the birefringence, $\Delta n$, increases regularly with draw.

At 50°C, the smectic phase is induced by the compression draw. The fraction of smectic phase increases rapidly (from 0 to 40%) for CR up to about 5, followed by a gradual increase[23]. This phase is considered to be 'soft' since the phase is a disordered form of α-crystal[40]. The results indicate that the existence of smectic phase reduces the tensile modulus in the plane direction. The smectic phase readily reverts back to the α-crystal phase by annealing above 70°C (ref. 27). The modulus for the annealed samples (140°C, 30 min) follows the same pattern as the samples prepared at 100 and 140°C, which possessed no smectic phase. *Figure 12* shows the tensile strength of these samples. The highest strength is 0.2 GPa, which is comparable to that of uniaxially drawn i-PP with a draw ratio of 6 (ref. 3). Elongation at break (~40% at CR = 30 (5.5 × 5.5)) is about twice that of uniaxially drawn i-PP at a comparable draw ratio of 6 (ref. 3).

*Layer structure*

*Figure 13* shows typical tensile stress–strain curves for samples with different CR values. The photograph is a sample after break (CR = 30). The fractured samples show delamination into a layered structure. This feature is most prominent for highly compressed samples. *Figure 14* shows a SEM photograph of a fracture surface. Many layers are seen. This layered structure induced by compression contrasts to the fibrillation found on uniaxial draw or to the fibril structures developed in the plane direction on biaxially drawn polyethylene gel films[8,11,14].

For further evaluation of structure, optical microscopy was performed. *Figure 15* shows polarized optical microphotographs of i-PP deformed at 140°C at the indicated CR. The plane of the photograph is parallel to the compression direction. As deformation proceeds, the spherulites assume a 'pan-cake' shape. At high CR, the layer structure is seen to be composed of a stacking of deformed spherulite planes. The shape of the deformed spherulite ('pan-cake') differs from the spheroid shape produced on uniaxial draw[41]. *Figure 16* is a schematic for the spherulite compression. If the deformation is affine, $CR = D_0/D$ (or $D = D_0 CR^{-1}$), where $D_0$ and $D$ are the diameters of uncompressed and compressed spherulites along the compression direction, respectively, and $CR = d_0/d_c$ is defined by the ratio of sample thickness before ($d_0$) and after ($d_c$) compression. *Figure 17* shows $D$ values as a function of $CR^{-1}$. The $D$ is evaluated from an average of 50 spherulites in the microphotographs. The relation between $D$ and $CR^{-1}$ is almost linear, implying virtually affine deformation. Therefore, the layer order and thickness can be controlled by the spherulite size of the original sample and the compression ratio.

The layered structure has a significant effect on impact toughness in the Bethlehem Steel Corporation process for making biaxially oriented polypropylene. Such sheet is sufficiently tough to stop bullets. Biaxially rolled i-PP

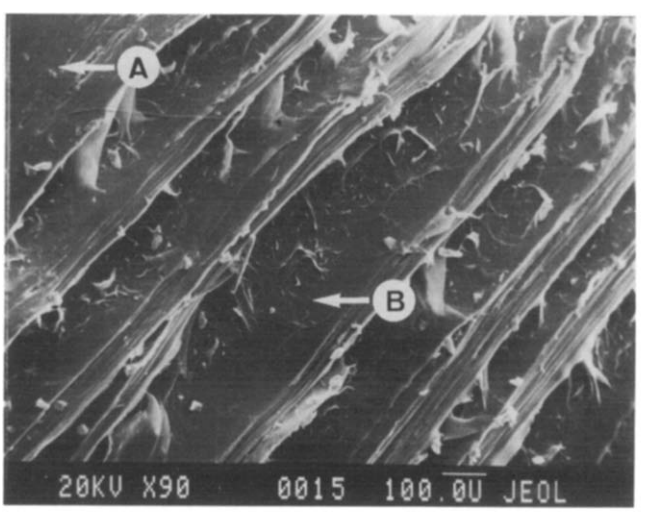


**Figure 14** SEM photograph of fracture surface for samples prepared at 50°C at CR = 9. The arrows A and B denote the sample surface and the layer surface, respectively

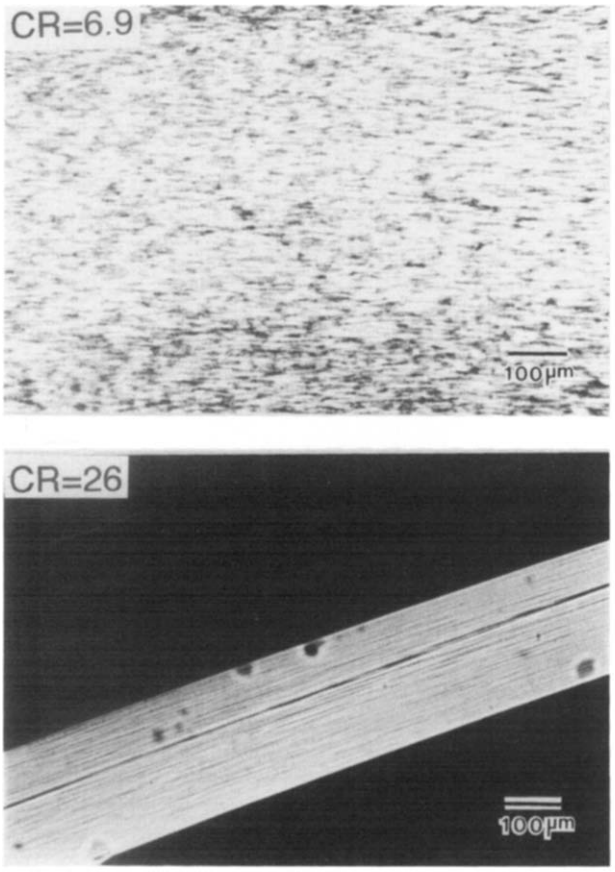


**Figure 15** Polarized optical microphotographs of samples prepared at 140°C at the indicated CR. The plane of the photograph is parallel to the compression direction

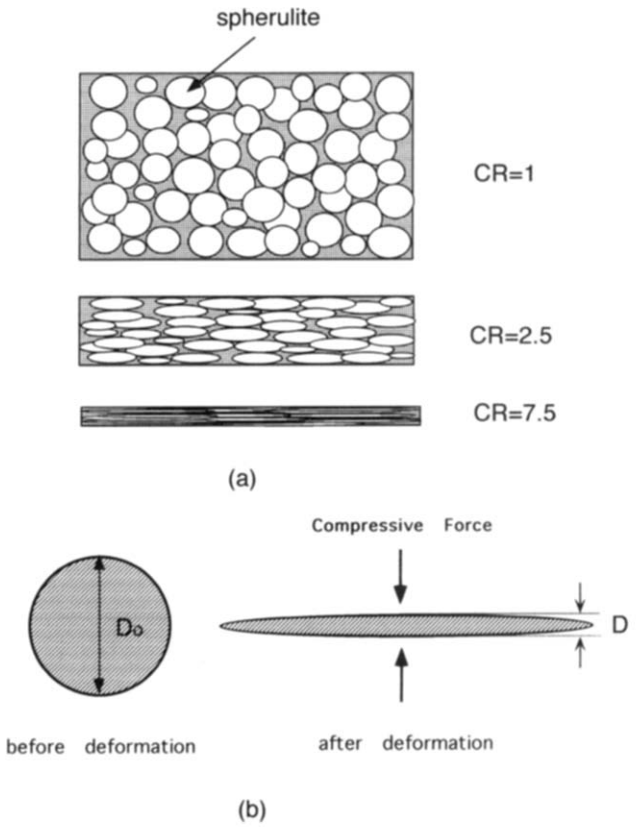


**Figure 16** Schematic of the compressed spherulites in macroscale (a) and on spherulite scale (b). $D_0$ is diameter of undeformed spherulite and $D$ is that of deformed spherulite along the compression direction

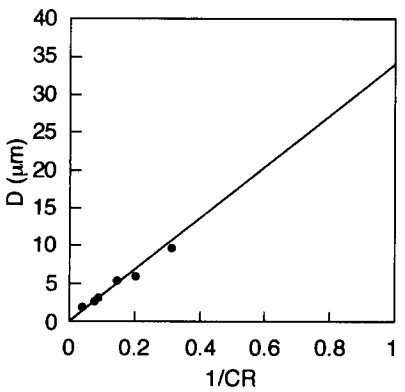


**Figure 17** Relation between $D$ and $CR^{-1}$

has also shown high impact strength (by Izod test); under certain conditions, the value is over 30 times higher than that of the original[42]. These increases in property perpendicular to the plane direction are much higher than increases in tensile strength along the plane direction (an increase of only a few times by compression biaxial draw). This may be related to the layer structure as well as to the planar chain orientation. If the impact is applied through the compression direction, the sample tends to rupture along the plane direction. The impact energy is absorbed by the tearing of many thin layers along the plane direction. The contact area of each deformed spherulite is also increased by draw (at CR = 50, the contact area is 50 times larger than that of the original). By these means, uniplanar deformed semicrystalline i-PP shows a remarkably high impact strength. Such a layer structure, caused by the compression draw, is also observed for highly compressed poly(4-methyl-1-pentene), high-density polyethylene, as well as non-crystalline polystyrene in our forging experiment.

## CONCLUSIONS

There are four major effects of planar deformation on the physical properties and morphology of i-PP. (1) The $T_g$ of the compressed sample increases with draw, due to the increase in amorphous density. (2) The smectic phase caused by the compression draw increases sample transparency. (3) Both tensile moduli and strengths parallel to the uniplanar direction increase with draw; the development of the smectic phase, however, reduces the tensile modulus with no significant effect on tensile strength. (4) The compressed samples exhibit a layered structure. The layer number and thickness can be controlled by the original spherulite size and subsequent compression.

## ACKNOWLEDGEMENT

Appreciation is expressed to the National Science Foundation for support through CUMIRP at the University of Massachusetts.

## REFERENCES

1 Zachariades, A. E. and Porter, R. S. (Eds) 'Strength and Stiffness of Polymers', Vol. 4, Plastic Engineering Series, Marcel Dekker, New York, 1983

2 Inoue, N. and Ichihara, M. (Eds) 'Hydrostatic Extrusion; Theory and Applications', Elsevier Applied Science, London, 1985
3 Kanamoto, T., Tsuruta, A., Tanaka, K. and Takeda, M. *Polym. J.* 1984, **16**, 75
4 Peguy, A. and Manley, R. St. J. *Polym. Commun.* 1984, **25**, 39
5 Matsuo, M., Sawatari, C. and Nakano, T. *Macromolecules* 1989, **22**, 2968
6 Adams, G. C. *J. Polym. Sci., Polym. Phys. Edn* 1971, **9**, 1235
7 Sakami, H., Iida, S. and Sasaki, K. *Kobunshi Ronbunshu* 1977, **34**, 653
8 Kaito, A., Nakayama, K. and Kanetsuna, H. *J. Appl. Polym. Sci.* 1984, **29**, 2347
9 Minami, S. and Itoyama, K. *Am. Chem. Soc. Polym. Prepr.* 1985, **26**, 245
10 Gerrits, N. S. J. A., Young, R. J. and Lemstra, P. J. *Polymer* 1990, **31**, 231
11 Gerrits, N. S. J. A. and Lemstra, P. J. *Polymer* 1991, **32**, 1770
12 Gerrits, N. S. J. A. and Young, R. J. *J. Polym. Sci., Polym. Phys. Edn* 1991, **29**, 825
13 Sakai, Y. and Miyasaka, K. *Polymer* 1988, **29**, 1608
14 Sakai, Y. and Miyasaka, K. *Polymer* 1990, **31**, 51
15 Sakai, Y., Umetsu, K. and Miyasaka, K. *Polymer* 1993, **34**, 318
16 Kyu, T., Fujita, K. and Cho, M. H. *Polym. Eng. Sci.* 1989, **29**, 383
17 Cakmak, M., Wang, Y. D. and Simhambhatla, M. *Polym. Eng. Sci.* 1990, **30**, 721
18 Cakmak, M. and Wang, Y. D. *J. Appl. Polym. Sci.* 1990, **41**, 1876
19 Taraiya, A. K., Orchard, G. A. J. and Ward, I. M. *J. Appl. Polym. Sci.* 1990, **41**, 1659
20 Higashida, Y., Watanabe, K. and Kikuma, T. *ISIJ Int.* 1991, **31**, 655
21 Vancos, G. J., Bruce, G. D. and Weatherly, G. C. *Polym. Commun.* 1990, **31**, 273
22 Mavridis, H., Bruce, G. D., Vancos, G. J., Weatherly, G. C. and Vlachopoulos, V. *J. Rheol.* 1992, **36**, 27
23 Osawa, S. and Porter, R. S. *Polymer* 1994, **35**, 545
24 Taraiya, A. K., Unwin, A. P. and Ward, I. M. *J. Polym. Sci., Polym. Phys. Edn* 1988, **26**, 817
25 Kaito, A., Nakayama, K. and Kanetsuna, H. *J. Macromol. Sci.-Phys.* 1987, **B26** (3), 281
26 Saraf, R. F. and Porter, R. S. *J. Rheol.* 1987, **31**, 59
27 Saraf, R. F. and Porter, R. S. *Polym. Eng. Sci.* 1988, **28**, 842
28 Samuels, R. J. *J. Appl. Polym. Sci.* 1981, **26**, 1383
29 Roy, S. K., Kyu, T. and Manley, R. St. J. *Macromolecules* 1988, **21**, 499
30 Kunugi, T., Ito, T., Hashimoto, M. and Ooishi, M. *J. Appl. Polym. Sci.* 1983, **28**, 179
31 Boyd, R. H. *Polymer* 1985, **26**, 323
32 McCrun, N. G. *J. Polym. Sci., Polym. Lett.* 1964, **2**, 495
33 Kawai, H., Hashimoto, T., Suehiro, S. and Fujita, K. *Polym. Eng. Sci.* 1984, **24**, 361
34 Simha, R. and Boyer, R. F. *J. Chem. Phys.* 1962, **37**, 1003
35 Van Krevelen, D. W. and Hoftyzer, P. J. 'Properties of Polymer, Their Estimation and Correlation with Chemical Structure', Elsevier Scientific, Amsterdam, 1976
36 Matsuo, M., Sawatari, C. and Nakano, T. *Polym. J.* 1986, **18**, 759
37 Cha, C., Moghazy, S. and Samuels, R. J. *Polym. Eng. Sci.* 1992, **32**, 1358
38 Brandrup, J. and Immergut, E. H. (Eds) 'Polymer Handbook', 3rd Edn, Wiley, 1989
39 Kunugi, T., Yoneyama, Y., Suzuki, A. and Porter, R. S. *J. Appl. Polym. Sci.* 1991, **43**, 429
40 Saraf, R. and Porter, R. S. *Mol. Cryst. Liq. Cryst. Lett.* 1985, **2** (3–4), 85
41 Samuels, R. J. 'Structured Polymer Properties', John Wiley and Sons, New York, 1974
42 Watanabe, K., Kanda, T., Higashida, Y. and Kikuma, T. Nippon Steel Corp., personal communication